Precambrian Research 231 (2013) 388–400

Contents lists available at SciVerse ScienceDirect

Precambrian Research

journal homepage: www.elsevier.com/locate/precamres

Stable isotope (S, C) chemostratigraphy and hydrocarbon biomarkers in the Ediacaran upper section of Sierras Bayas Group, Argentina

M. Bagnoud-Velásquez[a,*], J.E. Spangenberg[a], D.G. Poiré[b], L.E. Gómez Peral[b]

[a] Institute of Earth Sciences, University of Lausanne, 1015 Lausanne, Switzerland
[b] Centro de Investigaciones Geológicas, Universidad Nacional de La Plata-CONICET, calle 1 no. 644, 1900 La Plata, Argentina

ARTICLE INFO

Article history:
Received 8 August 2012
Received in revised form 28 March 2013
Accepted 1 April 2013
Available online xxx

Keywords:
Neoproterozoic
Sulfur isotopes
Hydrocarbon biomarkers
Trace elements
Water column stratification
Diagenesis

ABSTRACT

The Neoproterozoic sedimentary successions of the Sierras Bayas Group (SBG) are situated within the Tandilia Belt, Buenos Aires Province, Argentina. The Loma Negra Formation (LNF) from the upper part of the SBG has been investigated using a combination of inorganic, organic and isotopic geochemical methods in order to determine the stable isotope composition of carbonates ($\delta^{13}C_{car}$, $\delta^{18}O_{car}$), kerogen ($\delta^{13}C_{ker}$), pyrite and carbonate associated sulfur ($\delta^{34}S_{py}$, $\delta^{34}S_{CAS}$). Concentrations of major, trace and rare earth elements and hydrocarbon distributions were also investigated. This data set was used to further the understanding of the interactions between paleo-biodiversity and paleoenvironmental conditions for terminal Ediacaran (post-Gaskiers) shelf deposits. The high $\delta^{34}S_{py}$ values exceeding the coeval $\delta^{34}S_{CAS}$ values in green micritic limestones of the lower LNF may be explained by a combination of different events such as globally low seawater sulfate concentrations, an increased rate of bacterial sulfate reduction, and a decrease in sulfate levels in the near-bottom deepest water layer inherited from glaciations. Negative Ce anomalies in the dark grey micritic limestones of the upper LNF suggest they were deposited under oxidizing conditions. However, higher concentrations of Fe, Mo, Zn and REE, and the occurrence of authigenic ^{34}S-enriched pyrite suggest that the sediments were maintained under reducing conditions. The distributions of hydrocarbon biomarkers (e.g. hopanes maximizing at C_{29}) are in line with this hypothesis and indicate a diverse microbial community including primary producers such as cyanobacteria (e.g. terminally-branched monomethyl alkanes, hopanoid distribution), phototrophic bacteria (e.g. acyclic isoprenoids $C_{<21}$) and green bacteria (e.g. n-$C_{18} \gg$ Phytane). The unsteady $\Delta^{13}C_{car\text{-}ker}$ values reflect changes in primary biomass due to relative contributions of bacterial microorganisms using different photosynthetic carbon-fixation pathways. The lowest $\Delta^{13}C_{car\text{-}ker}$ values coincided with the latest biomarker signal interpreted as the signature of green non-sulfur bacteria using a less ^{13}C fractionation pathway. The combined biogeochemical features of the Loma Negra Formation, indicated a well-stratified water column with oxygenated surface waters, oxygen-poor bottom waters and anoxic sediments which helped to refine a correlation with the Polanco Formation from the Arroyo del Soldado Group in Uruguay.
© 2013 Elsevier B.V. All rights reserved.

1. Introduction

Carbon and sulfur isotope systems record processes such as the burial of sediments and the oxidation of environments, which in turn reflect the atmospheric oxygen levels and subsequently the chemistry of the ocean. The Neoproterozoic is recognized as a period of rapid buildup of atmospheric oxygen that coincided with deglaciation and early animal evolution (e.g. Kaufman and Hebert, 2003; Kaufman et al., 2007; Halverson et al., 2010). It is expected that these important changes would be followed by variations and heterogeneities in $\delta^{13}C$ and $\delta^{34}S$ values in different phases. The rise of oxygen in the Neoproterozoic likely allowed the oxidative episode of the sulfur cycle as well as the rapid diversification of animals in the Cambrian.

Due to the scarcity of sulfate minerals in Neoproterozoic sedimentary sequences, the record of $\delta^{34}S_{sulfate}$ is highly constrained. However, an alternative approach has been applied using structurally substituted carbonate-associated sulfate (CAS). Recent studies of $\delta^{34}S$ in sulfides and CAS have provided new insights about oxidized and reduced reservoirs (Hurtgen et al., 2002, 2004, 2005, 2006; Shields et al., 2004; Goldberg et al., 2005; Kaufman et al., 2007; Shen et al., 2008). The interval straddling the Precambrian–Cambrian boundary records extensive fluctuations in the $\delta^{34}S_{sulfate}$ values of evaporites, phosphorites (Shields et al., 2004) and CAS (Goldberg et al., 2005). These perturbations are explained by the presence of a marked vertical seawater $\delta^{34}S$

* Corresponding author. Present address: Environmental Engineering Institute – ENAC Faculty, EPFL, CH B2 397 – Station 6, Lausanne, Switzerland.
Tel.: +41 216936284.
E-mail address: Mariluz.Bagnoud@epfl.ch (M. Bagnoud-Velásquez).

0301-9268/$ – see front matter © 2013 Elsevier B.V. All rights reserved.
http://dx.doi.org/10.1016/j.precamres.2013.04.001

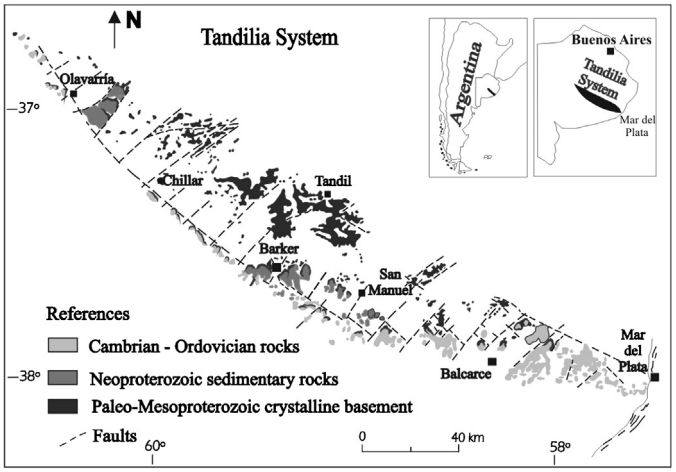

Fig. 1. Geological map of the Tandilia belt, Sierras Bayas Group, Argentina, South America (After Gómez Peral et al., 2007; Iñiguez Rodriguez, 1999).

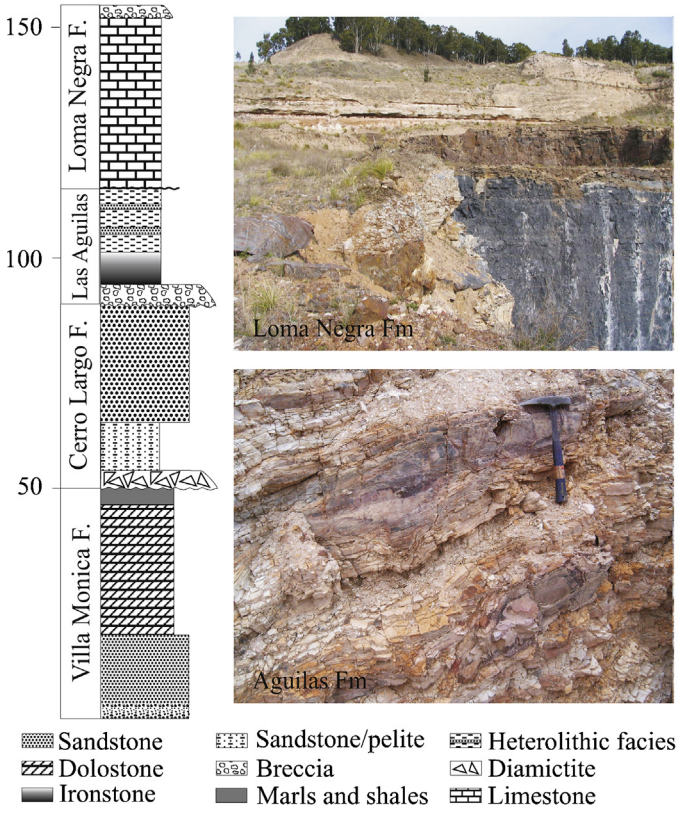

Fig. 2. Stratigraphic column of the Sierras Bayas Group (Argentina). Pictures show (from bottom to top): ironstones of the Las Aguilas Formation and limestones of the Loma Negra Formation with karstic breccias at the top.

gradient associated with low concentrations of oceanic sulfate (Hurtgen et al., 2004, 2006). Typical $\delta^{34}S_{sulfate}$ values until ~550 Ma are in the range of 15–30‰ (Hurtgen et al., 2005; Kaufman et al., 2007). Subsequently, extremely enriched $\delta^{34}S_{sulfate}$ values of ~40‰ were locally reported at the Precambrian–Cambrian boundary (Hurtgen et al., 2002). However, recent studies have indicated that seawater sulfate concentrations varied geographically and in some basins may have remained relatively low until around 551 Ma or until the Precambrian–Cambrian boundary (McFadden et al., 2008; Shen et al., 2008). A small sulfate reservoir coupled with a restricted basin, means that the isotopic composition of sulfate is more susceptible to external perturbations (Shen et al., 2008).

This paper presents the results of a combination of inorganic, organic and isotopic geochemical studies of the Ediacaran carbonate rocks of the Loma Negra Formation (Sierras Bayas Group), in the Barker area, Argentina. This work is part of an ongoing extensive biogeochemical correlation effort concerning Neoproterozoic to Cambrian deposits in SW-Gondwana, including the Corumbá Group (CG) in SW-Brazil, the Arroyo del Soldado Group (ASG) in Uruguay and the Sierras Bayas Group (SBG) in Argentina. These sedimentary successions were investigated using stable isotopes from carbonates ($\delta^{13}C_{car}$ and $\delta^{18}O$), their associated organic carbon ($\delta^{13}C_{ker}$) and sulfur species ($\delta^{34}S_{py}$ and $\delta^{34}S_{CAS}$), concentrations of major, trace and rare earth elements (REE), and the distribution of hydrocarbon biomarkers. Previous chemostratigraphic studies in the SBG were performed by Gómez Peral et al. (2007) in the NW-region of the Tandilia Belt. In this study, we provide new biogeochemical data in the central region of the belt (Fig. 1), with additional petrologic control through detailed petrographic and diagenetic analysis.

2. Geologic setting

The Sierras Bayas Group (SBG) is located in the Tandilia Belt, central part of the Buenos Aires province in Argentina (Fig. 1; Poiré, 1993). The Tandilia Belt is a NW-SE trending hill range approximately 350 km long, in the southern part of the Rio de la Plata Craton. It consists of an igneous-metamorphic Palaeoproterozoic basement with a Neoproterozoic to Early Paleozoic sedimentary cover. Palaeoweathering surfaces were observed between the crystalline basement and the sedimentary cover (Zalba et al., 1992).

The SBG (185 m) consists of four depositional sequences deposited in a shallow epicontinental sea and separated by regional unconformities (Poiré, 1993; Poiré and Spalletti, 2005; Poiré and Gaucher, 2009). From base to top, the SBG consists of the Villa Mónica, Cerro Largo, Las Aguilas (Barker area) which is equivalent to Olavarría (Sierras Bayas area) and Loma Negra formations (Fig. 2).

The Villa Mónica Formation (Poiré, 1993) is formed of quartz-arenites and arkosic sandstones at the base and dolostones including shallow marine stromatolites and shales at the top. The basal member is interpreted as a transgressive event (Poiré, 1993). Phosphates and hydrothermal pyrophyllite were reported at the top of the first quartz-arcosic facies association (Poiré et al., 2005; Gómez Peral et al., 2011). Martínez and Dristas (2007) confined the event to the contact and found evidence for a hydrothermal alteration model in which the unconformity acted as a hydrothermal channel. The stromatolite assemblage suggests a Riphean age (Poiré, 1993). Detrital zircon geochronology in sandstones shows a unimodal population of Palaeoproterozoic age indicating that they were derived from the underlying Buenos Aires Complex (Gaucher et al., 2008). Rapela et al. (2007) also report a minor detrital zircon age peak at ca. 1.0 Ga for this formation.

The Cerro Largo Formation (Poiré, 1993) is a siliciclastic, shallowing upward succession including from base to top a chert breccia, finely laminated glauconitc shale, fine-grained sandstone, cross-bedded quartz arenite, siltstone and claystone. This succession represents subtidal nearshore to shoreface deposits (Poiré, 1993). A diamictite was recently characterized at the base of the unit, including chert breccia (Colombo Diamictite; Poiré and Gaucher, 2009). If this diamictite unit has a glacial or a mass flow origin is still under consideration (Poiré, 2004; Poiré and Spalletti, 2005; Poiré and Gaucher, 2009; Gaucher and Poiré, 2009; Rapalini et al., 2013). Trace fossils reported by Poiré (1987), were re-interpreted as desiccation cracks associated to microbial mats (Porada and Bouougri, 2008). Detrital zircon geochronology in sandstones is characterized by a dominant Transamazonian population with peaks at 2.15, 2.0 and 1.78, but also displaying

Archaean-earliest Palaeoproterozoic (3.33, 2.99, 2.7, 2.46 Ga) and Mesoproterozoic peaks (1.55, 1.23 and 1.05 Ga) (Gaucher et al., 2008).

Las Aguilas Formation (Zalba, 1979) occurs at the Cuchilla de las Aguilas in the Barker area. From base to top four lithofacies are recognized: silicified calcareous breccias with oolites and peloids, ironstones, claystones and a coarsening upward, sandstone/shale heterolithic succession. The inferred environment for this unit is shallow marine with tidal influence (Dalla Salda et al., 2006). No glacial deposits are associated to the ferruginous lithologies (Poiré and Gaucher, 2009).

The Loma Negra Formation (Borrello, 1966) in the Barker area is composed of ~6 m of green and ~18 m of dark grey micritic limestones deposited in open marine ramp and lagoonal environments respectively (Poiré, 1993). The ramp could evolve to platform by the formation of a marginal barrier (Dalla Salda et al., 2006). Karstic breccias with development of phosphates mark a regional unconformity at the top of Loma Negra Formation pointing to a last regression in the basin and the platform subaerial exposition ("Barker surface"; Poiré and Gaucher, 2007; Gaucher and Poiré, 2009; Gómez Peral et al., 2011). This unit is also recognized in the Olavarria area.

The Ediacaran/Lower Palaeozoic Cerro Negro Formation (Iñiguez Rodriguez and Zalba, 1974) appears on top of this unconformity with palaeovalleys and positive relief. It is a 100–400 m thick unit characterized by reddish and greenish, brown olive claystones and heterolithic fine-grained sandstone–claystone interbeds, mainly formed in upper to lower intertidal flats. Detrital zircon U–Pb ages obtained from samples at the base of the unit show similar pattern reported for the Cerro Largo Formation with a minor population of Archaean zircon grains (Cingolani, 2011).

The occurrence of *Cloudina*, the trace fossil *Helminthopsis* sp. and probable medusa resting traces in the Loma Negra Formation suggest a late Ediacaran age (Poiré et al., 2003; Gaucher et al., 2005; Gaucher and Poiré, 2009). An acritarch assemblage dominated by *Leiosphaeridia* was characterized in Villa Monica Formation supporting also an Ediacaran age, in accordance with reported Sr isotopic data (Cingolani et al., 1991; Gaucher et al., 2005; Gómez Peral et al., 2007). Primary strontium isotope data between 0.7068 and 0.7075 support an Ediacaran age for the Loma Negra Formation (Kawashita et al., 1999; Gómez Peral et al., 2007). Finally, a stratigraphic correlation at formational level between SBG and Arroyo del Soldado Group (Uruguay) was proposed by Gaucher et al. (2005).

3. Samples and methods

3.1. Sampling

13 samples were collected in a quarry of the uppermost SBG covering siliciclasts of the Las Aguilas Formation ($n = 2$) and carbonates of the Loma Negra Formation ($n = 11$). One sample from the latter formation consisted of centimetric euhedral crystals of pyrite (carbonate matrix was not sampled). The studied section is from the central part of the Tandilia orographic belt, particularly from outcrops of the Villa Cacique Quarry (CIASA) in the Barker area, 90 km SE of the Olavarría-Sierras Bayas area (Fig. 1). These samples were selected for organic and inorganic geochemical analyses. Petrological and diagenetic analyses were developed over other 8 lime-mudstones samples from Loma Negra Formation in the same section.

3.2. Analytical methods

Samples were prepared and analyzed in the laboratories of the Institute of Earth Sciences at the University of Lausanne following procedures described by Spangenberg and Macko (1998), Spangenberg and Frimmel (2001) and Spangenberg and Herlec (2006). To remove the weathered material and any contamination from handling, the rock samples were cut in 2-cm-thick slabs with a water-cooled saw. These slabs were cleaned with distilled water and rinsed with analytical grade and glass distilled ethanol and dichloromethane, dried (50 °C for 24 h), crushed and powdered by short grinding periods in tungsten carbide ring grinder mill. An agate mill was used for preparation of aliquots for trace and rare earth elements analyses.

Carbon and oxygen isotope composition ($\delta^{13}C_{car}$ and $\delta^{18}O_{car}$) of whole rock carbonates from the Loma Negra Formation samples were determined using a Thermo Fisher carbonate-preparation device and Gas Bench II connected to a Delta Plus XL isotope ratio mass spectrometer (IRMS) that was operated in the continuous He flow mode. The CO_2 was extracted from carbonates with 100% phosphoric acid at 70 °C for calcite and 90 °C for dolomite. The stable C and O isotope ratios are reported in the delta (δ) notation as the per mil (‰) deviation relative to the Vienna Pee dee belemnite (VPDB) for carbon and Vienna Standard Mean Ocean Water (VSMOW) for oxygen. The analytical reproducibility estimated from replicate analyses of the laboratory standards Carrara marble and Binn dolomite was better than ±0.05% for $\delta^{13}C$ and ±0.1% for $\delta^{18}O$.

The samples were analyzed for major and trace elements (TE) by X-ray fluorescence analysis (XRFA) with a wavelength dispersive XRF-spectrometer (Philips® PW240) equipped with a 4 kW Rhodium X-ray tube. Major elements were analyzed using fused glass discs prepared with lithium tetraborate (1 g sample + 7 g $Li_2B_4O_7$). The detection limit for major elements is better than 0.01 wt%. Trace element analyses were performed in pressed pellets prepared with *Mowiol II* polyvinyl alcohol. The detection limit for trace elements is from 1 to 4 ppm. The rare earth elements (REE) were measured in the lithium tetraborate XRFA-discs by inductively coupled plasma-mass spectrometry (ELAN® 6100 DRC ICP-MS), calibrated with the SRM 612 trace element glass standards. The detection limit for the REE was from 0.02 to 0.15 ppm. The analytical reproducibility was better than ±5% for major and trace elements and ±10‰ for REE concentrations. The accuracies were of ±5‰ for all the elements.

Samples were submitted for total organic carbon (TOC) and Rock-Eval analyses at the Humble Geochemical Services Division (Shenandoah, TX). Total bitumen (extractable organic matter, EOM) was obtained from an aliquot (~200 g) of the powdered samples by refluxing with dichloromethane (DCM) for 6 days, with change of solvent after the first 2 days. The dichloromethane fractions were combined, let gently evaporate to 1 ml, and passed through an activated copper column to remove elemental sulfur. The solvent was passively evaporated to near dryness, and extracts with 0.5 ml DCM stored in 2 ml vials at +4 °C until required for analyses. The kerogen (organic matter insoluble in organic solvents, nonoxidizing acids and bases) was isolated from the extracted samples by HF–HCl treatment.

The separated kerogen was analyzed for carbon and nitrogen isotope composition ($\delta^{15}C$ and $\delta^{15}N$) by flash combustion on an elemental analyzer (Carlo Erba 1108 EA) connected to a Thermo Fisher Delta V IRMS (EA/IRMS). The $\delta^{15}C$ and $\delta^{15}N$ values are reported relative to VPDB and atmospheric nitrogen in air (N_2–air) standards, respectively. The reproducibility of the EA/IRMS measurements for carbon and nitrogen is better than ±0.1 and ±0.3%, respectively. The accuracy of analyses was assessed using international reference standards.

Carbonate-associated sulfate (CAS) was extracted from the bulk rock (cf. Burdett et al., 1989; Goldberg et al., 2005). The powder samples were leached for 24 h in 5.25% NaOCl to release sulfur, then washed three times with deionized water to remove soluble

sulfate. Leached powders were then put in solution with distilled 10 M HCl following a stepwise acidification procedure in which HCl acid was added successively 3 or 4 times. The supernatant of this solution, isolated before by gravity filtration, was heated near boiling to improve the reaction with saturated $BaCl_2$ added immediately. After 48 h reaction, the dissolved sulfate precipitated as barite and was recovered by centrifugation. Disseminated pyrite, present as euhedral to subeuhedral crystals in the micritic matrix of limestones, is not associated with veins and was directly extracted by micro-drilling. Sulfur isotope analyses were performed in the extracted CAS and in pyrites using an on-line elemental analyzer (Carlo Erba 1108) coupled through a continuous helium flow interface (ConFlo III) to a Delta S IRMS. The sulfur isotope values ($\delta^{34}S$) are reported relative to the Vienna Cañon Diablo Troilite (VCDT) standard. The analytical reproducibility for $\delta^{34}S$ values is better than ±0.2‰.

The organic matter extracts were separated into three fractions (aliphatic and aromatic hydrocarbons, NSO compounds) using silica/alumina gel liquid chromatography. Chemical characterization of the saturated hydrocarbons was performed with an Agilent Technologies gas chromatograph HP 6890 coupled to a HP 5973 quadrupole mass selective detector (GC-MSD), using a HP-5MS fused-silica capillary column (60 m length, 0.25 mm internal diameter, coated with 0.10 μm 5%-diphenyl–95%-dimethylpolysiloxane as stationary phase) and helium as carrier gas. The samples were introduced in a splitless injector at 280 °C. After an initial period of 7 min at 70 °C, the column was heated to 280 °C at 5 °C/min followed by an isothermal period of 20 min. The MSD was operated in the electron impact mode at 70 eV, source temperature of 250 °C, emission current of 1 mA and multiple-ion detection with a mass range from 50 to 700 amu. Compound identifications were made by comparison with synthetic standards, GC retention times, interpretation of mass spectrometric fragmentation patterns and literature mass spectra. The absence of measurable recovered bitumen in several blank runs indicates that no detectable laboratory contaminations were introduced into the samples.

4. Results

4.1. Petrography and diagenesis

4.1.1. Petrography

In the Barker area, the Loma Negra Formation is mostly composed of a micritic to microsparitic mosaic of low Mg calcite and less commonly shows sparitic texture (Fig. 3). This carbonatic mosaic commonly shows a xenotopic texture. Two types of microfacies were recognized: type 1 consists of green mudstones with a microlaminar structure, a planar and cross lamination with a lower $CaCO_3$ proportion (estimated by insoluble acid residue between 65 and 75%), and rich in clay-minerals (chlorite and illite) and in siliciclastic clasts (quartz and feldpars); and type 2 formed of microlaminated dark grey mudstones rich in $CaCO_3$ (80–90%) and in organic matter.

Detrital components are scarce and composed of quartz, feldspar, clay-minerals, and undifferentiated material. Quartz grains are either rounded or subrounded (Fig. 3), grouped and parallel to the stratification. Open space filling cements and authigenic minerals are very variable due to different extent of fracturation and circulation of diverse fluids within the poor porosity of the rock. The authigenic minerals in decreasing order of abundance are calcite (low Mg, high Mg and Fe-rich), chert, pyrite, and dolomite. Pyrite crystals have euhedral to subhedral shapes and vary in size from some microns to several milimeters (Fig. 3). Undifferentiated material is scarce and mostly disseminated between grains or in the stylolitic surfaces. In the top of the unit siliceous cementation is most frequently present as veins filled by chert. This cement also appears as replacement of calcite.

4.1.2. Diagenesis

Marine diagenesis is linked to the deposition of the micrite under a carbonatic ramp environment with the accumulation of green mudstones richer in detrital components. During the interaction with marine waters several crystals grew by aggradation and some dolomite crystals also occur as replacement into quartz grains (Fig. 3). Dark grey mudstones of the upper section of the unit were deposited under a restricted lagoon environment.

The well-preserved primary lamination and the sedimentary organic matter can be associated with microbial activity. Peloidal cement, internally composed by micritic calcite, shows pseudospherical forms with tens of microns. Authigenic pyrite crystals are frequent and were most probably formed by sulphate reduction during early diagenesis under anoxic to suboxic conditions. At the end of this stage a primary generation of calcite veins developed cutting perpendicularly to obliquely the primary lamination.

During burial the recrystallization of the non-planar micritic calcite started the development of a xenotopic mosaic of low Mg calcite by aggradation of the micritic matrix. However, microstructures and microbial laminations were almost unaffected by this process. Chemical compaction and stylolitization with concentration of residual minerals such as chlorite, illite, quartz and hematite, was observed. As a result of dissolution, stylolites present smooth profiles represented by low amplitude surfaces. A second dissolution stage is recognized during this regime by the generation of secondary porosity as veins and vugs which are later occluded by calcite cements. This second generation of veins crosscuts the first generation mentioned above.

4.2. Stable isotopes of carbon and oxygen in carbonates

The oxygen isotope composition of Loma Negra limestones ranges between −6.6 and −12.7‰ VPDB (Table 1). These $\delta^{18}O_{car}$ values are mostly in the range of unaltered values (Fölling and Frimmel, 2002). No positive correlation between $\delta^{13}C_{car}$ and $\delta^{18}O_{car}$ is observed; on the contrary, they exhibit a negative correlation ($r = -0.6$; Fig. 4). The $\delta^{13}C_{car}$ values are thus suitable for evaluating the primary seawater carbon isotopic composition.

The stratigraphic variation of $\delta^{18}O_{car}$ values follows the main lithological variations as also reported in the Olavarría area (Fig. 4, Gómez Peral et al., 2007). For instance, Gómez Peral et al. (2010) remark that $\delta^{18}O$ stratigraphic excursions (from −7.4 to −13.5‰) show a regional connotation in the Tandilia System, and should be associated with a primary signature. Thus, the gradual increase in $\delta^{18}O$ values observed ubiquitously in the Tandilia system could be a primary feature of global cooling.

The carbon isotope values in the Loma Negra limestones vary from 2.3 to 4‰ VPDB (Table 1). The lowest $\delta^{13}C_{car}$ values are recorded toward the top of the section and higher values in the transition between green and black limestones. They are consistent with isotope data reported by the authors in correlative limestones of the lower-middle Polanco Formation (Arroyo del Soldado Group) in Uruguay (Bagnoud, 2010; Gaucher et al., 2004; Gaucher et al., 2009; Frei et al., 2011) and in the Tamengo Formation (Corumbá Group) in Brazil (Bagnoud, 2010; Gaucher et al., 2003; Boggiani et al., 2010) as well as with values reported in the Olavarría area (Gómez Peral et al., 2007).

4.3. Major, trace and rare earth elements

The major element concentrations were analyzed in order to determine the variations in the carbonate content and the amount of siliciclastic components. The correlation of Al_2O_3 concentration

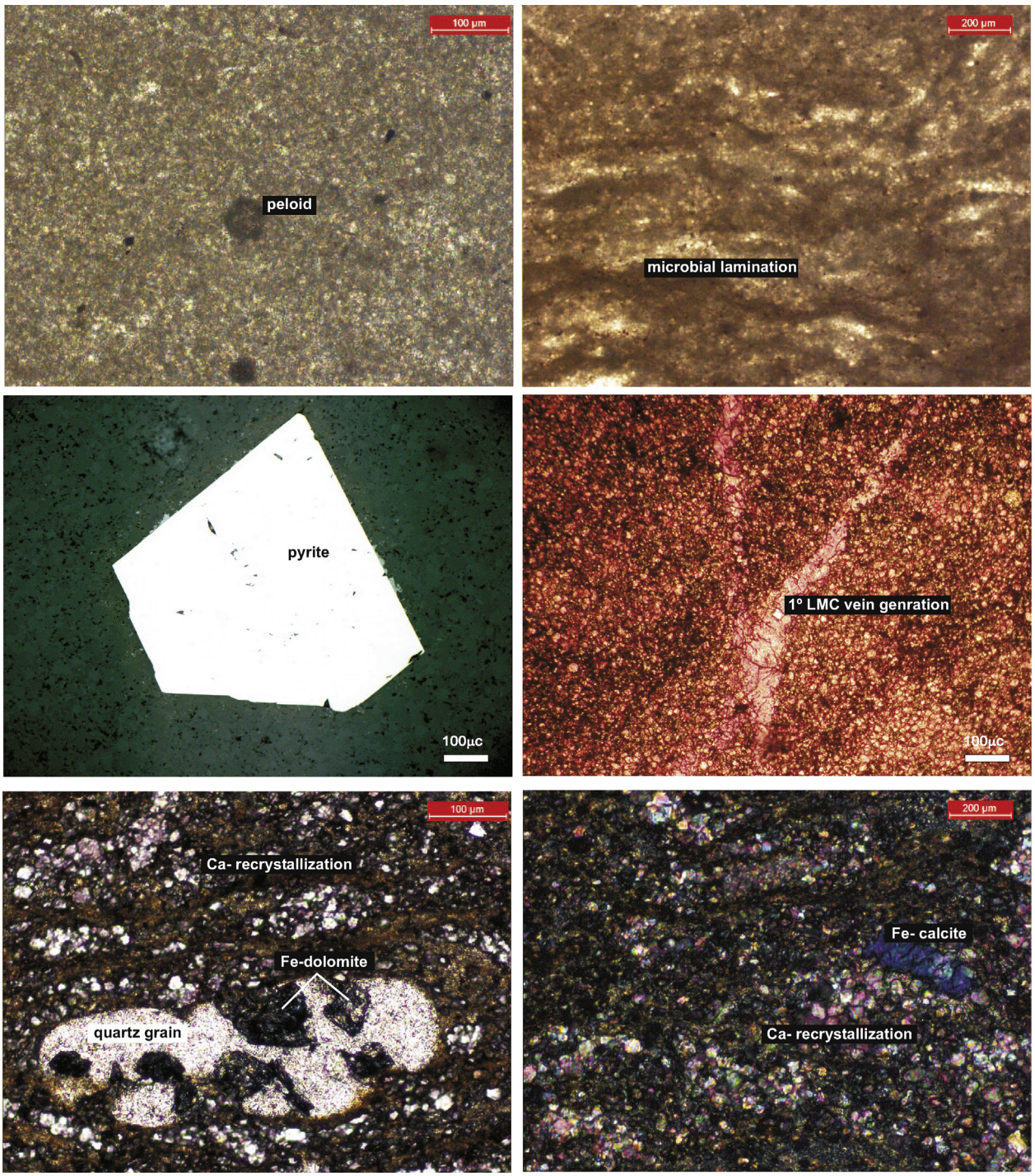

Fig. 3. Photomicrographs of selected mud–limestones samples from Loma Negra Formation showing main mineralogical components (detrital and authigenic). LMC, low magnesium calcite; Ca, calcite; Fe, iron.

with the other major elements can be used as a proxy for a siliciclastic origin (Veizer, 1983). Al_2O_3 is positively correlated with SiO_2, TiO_2, Fe_2O_3, MgO, Na_2O and K_2O and moderately with P_2O_5 indicating that these elements are associated with detrital phases (Table 2). MnO and CaO are negatively correlated with Al_2O_3 explaining their relationship with carbonate production. The Fe_2O_3 content is significant at the top of the Las Aguilas Formation and in the green micritic limestones at the lower Loma Negra Formation, with values ranging between 3024 and 28,266 ppm (Table 1). This increase in the green limestones coincides with high values in carbon and sulfur isotopic ratios as well as with the occurrence of disseminated pyrite (Fig. 4). A decrease in Fe_2O_3 content is evident up-section in the black micritic limestones.

Concentrations of total Fe and Mn were normalized to Al, while Mo, V, U, Ni, Zn and Pb concentrations were normalized to Th. All of them were compared to average carbonate baseline (Turekian and Wedepohl, 1961) and are shown in Fig. 4. Both, Fe/Al and Mn/Al ratios remain below the average carbonate values with the exception of a sample at the base of Loma Negra Formation showing a higher Fe/Al value. Most of the trace elements normalized to Th (TE/Th ratios) show values above the average carbonate value in

Table 1
Major, trace, rare earth element contents and stable isotopes of the Sierras Bayas Group samples.

Sample		AR01	AR02	ARP7	AR04	AR05	AR06	AR07	AR08	AR09	AR10	AR11	AR12
Description		P	P	L	L	L	L	L	L	L	L	L	L
Distance to the base (m)		15	22	25	29	31	34	39	44	49	52	55	58
SiO_2	wt%	63.41	58.32	12.71	28.93	29.82	14.2	11.56	7.84	9.25	9.09	12.29	10.25
TiO_2	wt%	0.69	0.62	0.06	0.2	0.23	0.06	0.06	0.04	0.04	0.03	0.04	0.04
Al_2O_3	wt%	14.54	13.61	1.21	4.4	4.95	1.23	1.28	0.7	0.74	0.6	0.76	0.72
Fe_2O_3	wt%	8.08	7.22	0.86	3.46	2.83	1.02	0.63	0.56	0.29	0.47	0.46	0.47
MnO	wt%	0.02	0.01	0.07	0.05	0.04	0.06	0.06	0.05	0.05	0.06	0.09	0.1
MgO	wt%	1.81	1.48	0.28	0.57	0.62	0.6	0.27	0.29	0.31	0.18	0.22	0.2
CaO	wt%	1.61	5.96	46.99	33.8	32.91	45.98	47.89	50.14	49.96	49.32	48.04	49.21
Na_2O	wt%	0.08	0.09	0.04	0.04	0.04	0.03	0.02	0.03	0.03	0.03	0.02	0.03
K_2O	wt%	4.97	5.08	0.25	1.69	1.84	0.33	0.34	0.16	0.1	0.09	0.14	0.18
P_2O_5	wt%	0.15	0.11	0.03	0.12	0.1	0.1	0.04	0.04	0.04	0.04	0.05	0.04
LOI	wt%	4.87	7.80	37.24	26.94	26.59	36.62	37.99	39.87	39.35	39.29	37.93	38.76
Sc	ppm	27.14	22.94	3.94	3.05	9.81	15.37	3.61	5.00	3.77	3.50	3.41	4.11
V	ppm	73.1	54.5	16.0	7.4	21.2	31.9	10.2	16.2	9.6	10.1	12.8	12.1
Cr	ppm	90.4	75.7	6.7	11.4	23.5	35.6	11.0	11.2	9.2	7.6	8.3	7.7
Mn	ppm	71	146	534	394	284	492	433	418	376	468	668	759
Fe	ppm	25,255	28,266	3024	12,099	9883	3551	2214	1952	1019	1647	1595	1649
Co	ppm	11.9	10.5	1.4	1.2	5.0	7.6	1.6	2.0	4.2	1.6	1.8	1.4
Ni	ppm	35.5	28.2	3.4	3.6	12.9	17.2	4.4	7.4	8.6	4.7	7.1	5.0
Cu	ppm	35.0	30.9	10.0	8.5	8.9	33.6	12.1	12.5	7.6	10.9	10.1	12.9
Zn	ppm	129.1	107.4	37.1	22.2	42.8	62.6	28.6	59.2	68.8	63.4	63.7	55.6
Ga	ppm	20.9	19.2	1.1	1.3	5.9	9.4	1.8	1.8	1.1	1.2	0.9	1.3
As	ppm	1.1	2.9	1.0	0.4	0.6	1.3	1.1	1.8	1.2	2.2	2.0	0.9
Rb	ppm	203.0	207.4	6.2	7.1	60.5	96.1	12.4	12.4	5.4	4.1	4.0	5.9
Sr	ppm	137	202	281	224	398	586	474	282	284	270	300	312
Y	ppm	36.5	25.6	15.0	8.9	16.3	26.0	7.6	16.8	12.1	11.3	13.7	15.5
Zr	ppm	139.0	117.4	6.1	7.7	38.3	64.1	12.3	11.3	6.7	6.4	5.3	7.0
Nb	ppm	11.95	10.78	0.52	0.68	3.36	5.68	1.08	1.01	0.55	0.57	0.52	0.64
Mo	ppm	0.58	0.47	0.35	0.33	0.31	0.29	0.31	0.36	0.26	0.22	0.31	0.34
Cs	ppm	10.04	9.03	0.17	0.24	2.12	3.10	0.32	0.34	0.19	0.13	0.14	0.17
Ba	ppm	1131	1177	188	368	478	851	219	114	104	306	131	137
Ce/Ce*		0.95	0.92	0.63	0.65	0.86	0.85	0.81	0.59	0.58	0.71	0.49	0.51
$\sum REE_{PAAS}$	ppm	14.6	19.1	4.7	3.0	7.1	11.7	3.0	5.7	4.1	4.0	4.4	5.0
Hf	ppm	4.0	3.4	0.2	0.2	1.1	1.8	0.4	0.3	0.2	0.2	0.1	0.2
Ta	ppm	0.91	0.85	0.04	0.06	0.25	0.44	0.08	0.09	0.05	0.04	0.03	0.06
Pb	ppm	11.9	18.2	0.9	1.1	5.6	7.3	1.7	1.8	10.9	1.0	0.7	0.9
Th	ppm	14.73	13.00	0.77	0.92	4.11	7.20	1.20	1.27	0.82	0.69	0.68	0.85
U	ppm	1.39	1.14	0.16	0.14	0.36	0.57	0.24	0.24	0.12	0.15	0.14	0.14
$\delta^{13}C_{car}$	‰, VPDB	1.2	−2.4	3.7	3.9	3.9	3.3	4.0	3.2	2.3	2.4	2.3	2.5
$\delta^{13}C_{ker}$	‰, VPDB	−26.8	−25.5	−26.9	−23.3	−26.05	−22.77	−23.6	−24.2	−25.4	−24.4	−23.4	−22.8
$\Delta^{13}C_{car\text{-}ker}$	‰, VPDB	28.0	23.0	30.6	27.2	29.9	26.0	27.7	27.4	27.7	26.8	25.7	25.3
$\delta^{13}C_{eom}$	‰, VPDB	−27.7	−29.2	–	−27.9	−29.0	−27.8	−27.0	−27.2	−28.1	−28.2	−28.0	−28.1
$\Delta^{13}C_{ker\text{-}EOM}$	‰, VPDB	0.9	3.8	–	4.6	3.0	5.0	3.4	3.0	2.7	3.8	4.6	5.3
$\delta^{18}O_{car}$	‰, VPDB	−12.8	−12.8	−11.7	−12.6	−12.7	−11.8	−8.1	−6.9	−6.6	−6.7	−8.6	−9.3
$\delta^{34}S_{py}$	‰, CDT	13.2	–	24.2	30.6	30.1	32.5	–	–	–	–	–	–
$\delta^{34}S_{CAS}$	‰, CDT	–	–	25.6	28.4	28.9	27.7	24.6	24.5	24.2	25.2	25.8	25.1

P, pelites; L, limestones.

samples from the Loma Negra Formation, at the base and in the black micritic limestones. The latter are characterized by a progressive increasing trend, with higher values at the top. The U/Th and Ni/Th ratios have values lower than the average carbonate values but they follow a similar trend compared with the other ratios.

Rare earth elements (REE) contents were normalized with Post-Archaean Average Shale (PAAS) composition (Taylor and McLennan, 1985). The REE distribution profiles are mostly flat for the pelites and for the green limestones of the Las Aguilas and Loma Negra formations respectively while the upper facies (black limestones of Loma Negra Formation) records some little variations

Table 2
Correlation matrix of major elements in samples from the SBG.

	SiO_2	TiO_2	Al_2O_3	Fe_2O_3	MnO	MgO	CaO	Na_2O	K_2O	P_2O_5
SiO_2	1.00									
TiO_2	0.99	1.00								
Al_2O_3	0.99	1.00	1.00							
Fe_2O_3	0.99	0.99	0.99	1.00						
MnO	−0.79	−0.80	−0.81	−0.80	1.00					
MgO	0.97	0.98	0.97	0.97	−0.80	1.00				
CaO	−1.00	−1.00	−1.00	−1.00	0.79	−0.98	1.00			
Na_2O	0.95	0.96	0.96	0.95	−0.79	0.93	−0.95	1.00		
K_2O	1.00	1.00	1.00	0.99	−0.81	0.97	−1.00	0.96	1.00	
P_2O_5	0.84	0.79	0.79	0.84	−0.67	0.83	−0.83	0.69	0.80	1.00

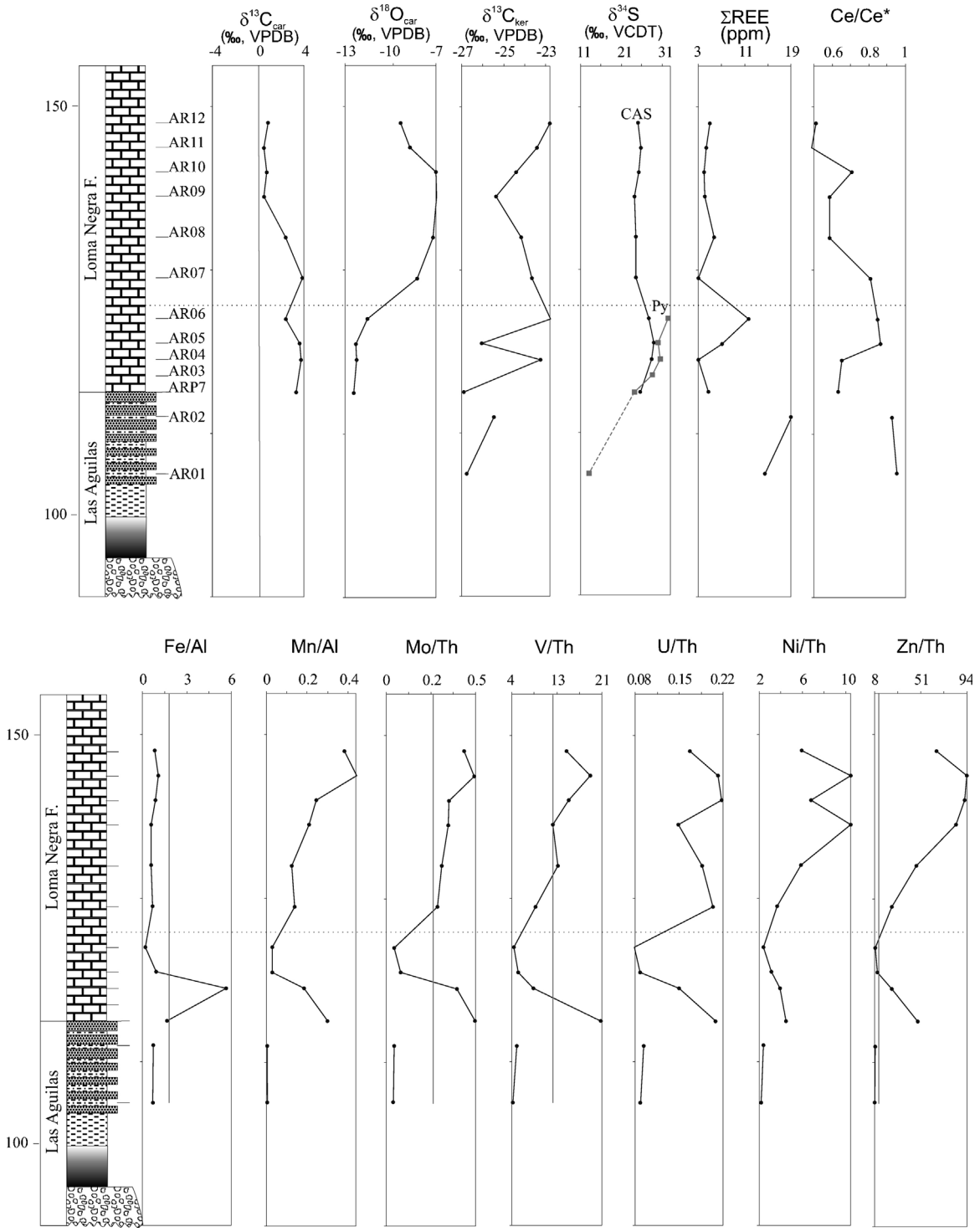

Fig. 4. Geochemical profiles of stable isotopes ($\delta^{18}O_{car}$, $\delta^{13}C_{car}$, $\delta^{13}C_{ker}$, $\delta^{34}S_{py}$ and $\delta^{34}S_{CAS}$), Ce anomaly and concentrations of selected redox-trace and rare-earth elements in samples from the SBG. The dotted horizontal line through all profiles indicates the division between the green (below) and black (above) limestones of Loma Negra Formation. The average carbonate baseline (Turekian and Wedepohl, 1961) is indicated as a vertical line for the elemental profiles.

(Fig. 5). The latter also record the lowest REE concentrations. The flat trend in the REE distributions of the lower facies is mostly due to its shale content. A slightly negative Ce anomaly is well pronounced in the upper black limestones of Loma Negra Formation (Fig. 5). Conversely, no Eu anomalies are evident in these samples. Values for PAAS-normalized Ce anomaly range between 0.49 and 0.95 with values distant to the unit characterizing the black micritic limestones (Fig. 4 and Table 1). This is equally noted in the REE distribution patterns.

4.4. Sulfur isotopes in carbonate-associated sulfate and pyrite

The $\delta^{34}S_{CAS}$ values range between 24.2 and 28.9‰ VCDT while the limited $\delta^{34}S_{py}$ data in finely disseminated pyrite range between 13.2 and 32.5‰ (Table 1). The $\delta^{34}S_{CAS}$ values are lower than the $\delta^{34}S_{py}$ values excepting for one sample at the base of Loma Negra Formation showing an inversed trend (Fig. 4). The measured sample from the Las Aguilas Formation is characterized by the lowest $\delta^{34}S_{py}$ value; then, a progressive increase is recorded in the green

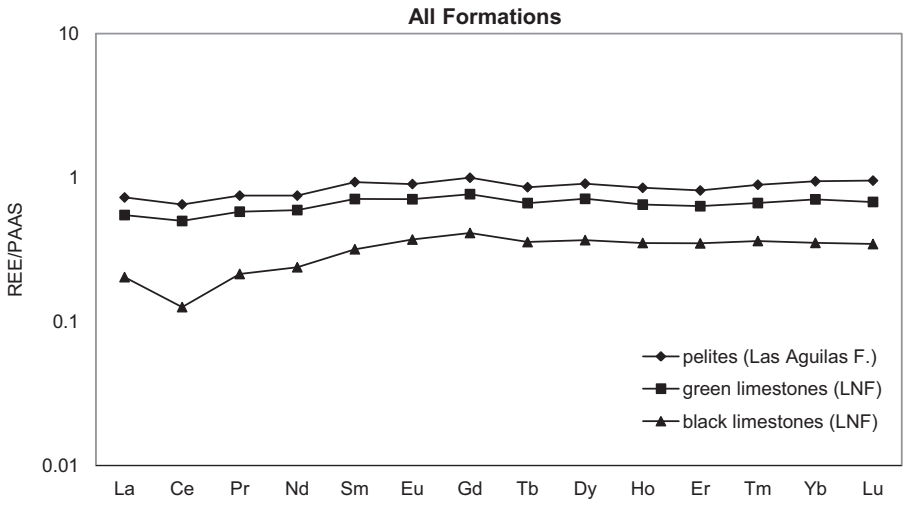

Fig. 5. Average PAAS normalized REE patterns of different studied lithologies of SBG.

micritic limestones of the Loma Negra Formation and finally a small depletion is evident upward in the black micritic limestones but the $\delta^{34}S_{CAS}$ values remain constant until the top of the section (Fig. 4). No pyrite was recorded in the black micritic limestones of the Loma Negra Formation. Pyrite in the green limestones of Loma Negra Formation is recorded as disseminated euhedral to subeuhedral crystals and their emplacement in the micritic limestones is never associated with veins. In this way, pyrite is considered authigenic and should reflect the environment of deposition. Sulfur isotopic composition of sulfide ($\delta^{34}S_{py}$) and coeval CAS ($\delta^{34}S_{CAS}$) is similar exhibiting a covariation (Fig. 4). In addition, the similarity of the $\delta^{34}S_{py}$ and $\delta^{34}S_{CAS}$ patterns with the $\delta^{13}C_{car}$ stratigraphy is remarkably (Fig. 4).

The validity of the sulfur isotope data needs to be assessed since experiments have demonstrated that oxidation of pyrite can occur during laboratory extraction of CAS (Shen et al., 2008). If both sulfate and Fe were retained in the rock and later liberated in CAS extraction, a strong positive correlation between them is expected. However, our data show a weak correlation between $\delta^{34}S_{CAS}$ and [Fe] arguing against contamination from pyrite oxidation (Fig. 6).

4.5. Bulk isotopic composition of kerogen

The $\delta^{13}C_{ker}$ values from samples of the uppermost SBG cover a narrow range of −26.9 to −22.8‰ VPDB (Table 1). The lowest $\delta^{13}C_{ker}$ values are recorded in the Las Aguilas Formation as well as in some green micritic limestones at the base of Loma Negra Formation. Therefore, the latter facies record fluctuating $\delta^{13}C_{ker}$ values encompassing also the most ^{13}C enriched kerogen (Fig. 4). The two topmost samples of the section show ^{13}C-enriched kerogen as well. The isotopic difference between carbonate and associated kerogen ($\Delta^{13}C_{car\text{-}ker}$) ranges from 25.3 to 30.6‰; the highest values are recorded by green micritic limestones at the Loma Negra Formation (Table 1). This range is consistent with carbon isotope fractionation by oxygenic photoautotrophs. Both, $\delta^{13}C_{car}$ and $\delta^{13}C_{ker}$ signatures have a coupled behaviour for most of the section arguing against a diagenetic origin (Fig. 4).

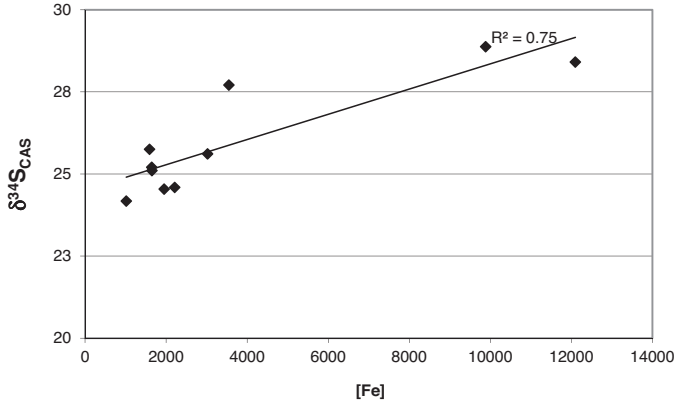

Fig. 6. Cross-plot of [Fe] vs. $\delta^{34}S_{CAS}$ values from samples of Loma Negra Formation, SBG.

4.6. Molecular composition of the Loma Negra bitumen

The extracted hydrocarbons are evaluated to determine if they are truly syngenetic through comparison of the carbon isotopic compositions of kerogen and bitumen fractions. The kinetic fractionation decreases with the polarity of organic fractions: $\delta_{ker} > \delta_{EOM}$ (Schoell, 1984). Our data follow this trend with δ_{ker} average values of −24.3 and δ_{EOM} average values of −27.9‰ VPDB for the Loma Negra samples. The indigenous nature of the different organic matter fractions is in this sense confirmed (Table 1).

GC–MSD total ion chromatograms of the saturated hydrocarbons in all the samples from the Loma Negra Formation are closely similar. They are characterized by unimodal distributions of homologous series of *n*-alkanes in the C_{13}–C_{30} range with common maxima at C_{20} (Fig. 7). The predominance of *n*-C_{20} indicates an input of algal-bacterial lipids (Volkman et al., 1980). The carbon preference index (CPI, calculated as total odd/total even over full carbon number range) ranging from 0.91 to 1.06 indicates that no odd/even C-number predominance characterizes the *n*-alkanes series (Table 3). Monomethylalkanes occur between *n*-C_{17} and *n*-C_{21} with a dominance of 2- and 3-Me alkanes suggesting a cyanobacterial source (Shiea et al., 1990). A heterotrophic bacterial source was suggested for 2-methylpentadecanes and a methanogenic source for 2-methyloctadecanes (Ten Haven et al., 1988; Brassell et al., 1981 respectively). Acyclic isoprenoids of less than 21 carbons including pristane and phytane are present, confirming the contribution of phototrophic bacteria. Pristane (Pr) and Phytane (Ph) can be derived from the phytol side-chain of chlorophyll in aerobic phototrophic organisms such as algae and cyanobacteria or from bacteriochloropylls *a* and *b* of phototrophic bacteria. A predominance of *n*-C_{18} over phytane is evident in some samples (Table 3 and Fig. 7). This feature is noticed also in anoxygenic photosynthetic bacterial mats dominated by green bacteria

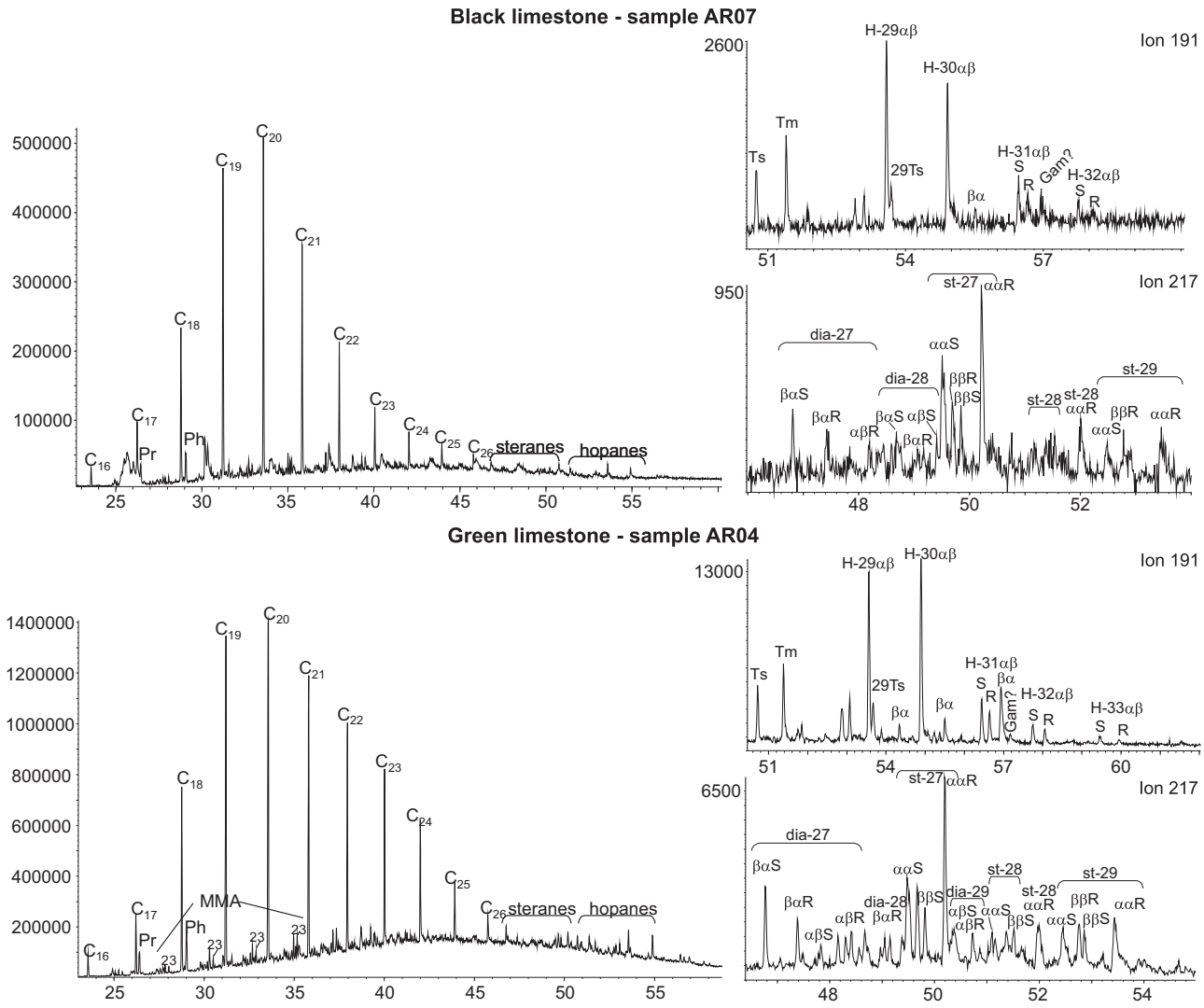

Fig. 7. Total ion current chromatogram (TIC) and distribution of hopanes (*m*/*z* 191) and steranes (*m*/*z* 217) of aliphatic hydrocarbons in representative samples from the SBG. *Abbreviations*: x = C number; Cx = *n*-alkanes with x C number; Pr = Pristane; Ph = Phytane; H-xαβ = 17α(H) 21β(H)-hopanes; βα = 17β(H) 21α(H)-hopanes, S and R epimer configuration at C-22; Tm = 17α(H)-22, 29, 30-trisnorhopane; 27β = 17β(H)-trisnorhopane; 29Ts = 18α(H)-30-norneohopane; dia-x = diasteranes with x C number; st-x = steranes with x C number.

(Shiea et al., 1991). Homologous series of alkylcyclohexanes were identified in the range C_{16}–C_{25}, with maxima at C_{21} (Fig. 7). Alkylcyclohexanes could be the diagenetic cyclization products of acyclic polymethylenic precursors (Gelin et al., 1994). Cyclohexyl fatty acids from bacteria (Oshima and Ariga, 1975; Volkman et al., 1980) or algae (Schulze and Michaelis, 1990) have been suggested as potential precursors for alkylcyclohexanes.

Hopanes (*m*/*z* 191) and steranes (*m*/*z* 217), hydrocarbon biomarkers of bacteria and algae respectively (Peters et al., 2005), were also detected in these samples. The hopanes/steranes concentration ratio (Hop/Ster) indicates the prokaryotic versus eukaryotic input to the sedimentary organic matter. These samples have a Hop/Ster ratio of 1.5 indicating a predominance of prokaryotic input (Fig. 7). Extended C_{29}–C_{34} hopanes (homohopanes) in these samples are compounds synthesized by bacteria not strictly anaerobic (Ourisson and Albrecht, 1992). Some black limestone samples exhibit hopane series maximizing at C_{29} (e.g. sample AR07). This distribution indicates an anoxic source-rock depositional setting (Peters et al., 2005). C_{27}–C_{29} steranes indicate an input from eukaryotes.

5. Discussion

5.1. Diagenetic constraints

Petrographic and diagenetic studies were recorded for Loma Negra Formation in the Olavarría area (Gómez Peral et al., 2007, 2010), but no previous results are known from the central area of Tandilia System up to the present work. In the Barker area, the Loma Negra Formation is petrographically characterized by the presence

Table 3
Distribution of hydrocarbons and selected biomarkers parameters in samples from the SBG.

Samples	*n*-Alkanes (max.)	CPI	Pr/Ph	Pr/*n*-C_{17}	Ph/*n*-C_{18}
Red limestones	C_{13}–C_{30} (C_{20}, C_{21}, C_{25}, C_{26})	0.91–1	0.38–0.81	0.59–1.76	0.49–1.48
Black limestones	C_{13}–C_{26} (C_{20})	1.06	0.61–1.01	0.67–0.89	0.32–0.41

of two types of microfacies that are differentiated by their variable contents of terrigenous grains (quartz, feldpars, clay-minerals) and organic matter. During deposition and also early marine diagenesis, it appears that the dominant processes were the precipitation of micritic peloidal cement and authigenic growth of pyrite. The organic matter and the primary microbial lamination show high degree of preservation. The early fluid interaction favoured a first stage of dissolution-vein generation filled by sparitic calcite cement and less commonly by chert.

Early to intermediate burial diagenesis is associated to neomorphism-aggradation of the primary calcite crystals, chemical compaction and stylolitization. A second stage of dissolution-vein generation with later calcite cementation and the transformation of chert to micro- and mesoquartz were also recognized. It is important to remark that burial diagenetic processes were not generalized and a high degree of preservation of the primary texture is recognized which make this unit different from other Neoproterozoic sections of SW-Gondwana (Misi et al., 2007; Gómez Peral et al., 2007; Frimmel, 2010, and herein)

Petrographic and diagenetic evidence as well as the elemental and isotopic composition of these rocks at the Barker location, point to a pristine chemical composition as discussed above for every diagenesis-sensitive parameter. A low water/rock ratio could explain the persistence of a uniform geochemical distribution within the characteristic values for low-grade diagenetic alteration.

5.2. Implications of combined geochemical proxies

One of the most significant signatures displayed by the Loma Negra Formation (SBG) chemostratigraphic data is the ^{34}S enrichment in pyrite related to coeval trace sulfate and its coincidence with relatively enriched carbon isotopic values in the green micritic limestones package. Carbon and sulfur isotope ratios are characterized by the most highly enriched values along the section. It is asserted that the formation of sedimentary pyrite occurs in anoxic environments where bacterial sulfate reduction takes place and reactive iron supply is available. Bacterial sulfate reduction involves significant isotopic fractionation and sedimentary pyrite is thus expected to be lighter than contemporaneous seawater sulfate (Canfield and Thamdrup, 1994). However, an inversed situation was commonly reported in several works dealing with Neoproterozoic sediments (e.g. Hurtgen et al., 2002; Habicht et al., 2002; Strauss, 2002; Lyons et al., 2006; Shen et al., 2008; Ries et al., 2009; Reuschel et al., 2012). Only some of these studies provide an explanation for the striking $\delta^{34}S_{py}$ values (exceeding coeval $\delta^{34}S_{CAS}$) using a model where sulfate concentrations were very low (e.g. Ries et al., 2009). Neoproterozoic oceanic sulfate concentrations were indeed on average much lower than modern values, ca. 3 mM (Hurtgen et al., 2004). Ries et al. (2009) attributed that they called "superheavy pyrites" to an exceptional low sulfate concentration in the ocean coupled with enhanced bacterial sulfate-reduction.

In order to better understand the source of the ^{34}S-enriched pyrite in the Loma Negra limestones, the behaviour of the whole measured geochemical parameters is considered. High Fe concentrations and peak values above the average carbonate baseline for Fe_T/Al, Mo/Th and Zn/Th as well as high $\sum$REE contents and no clear Ce anomaly were observed in the green micritic limestones (Fig. 8). In general, high concentrations of Fe, Mo, Zn and REE with the occurrence of authigenic pyrite are all in line with reducing conditions and associated metal recycling. Iron is remobilized from oxic shelves and scavenged from the anoxic to euxinic water column during authigenic pyrite formation in the contact of redox chemocline with sediments or close to the sediment–water interface (Lyons et al., 2003). This process can be recognized by high Fe_T/Al ratios indicating enrichments in reactive iron. The existence of a redox stratified ocean is thus clear from these results and

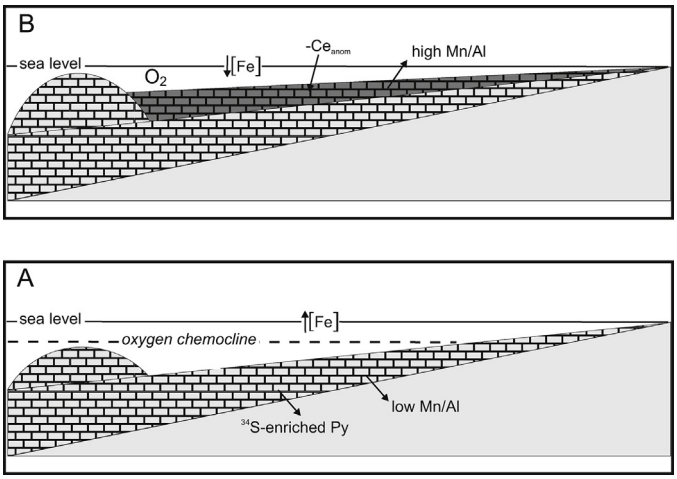

Fig. 8. Biogeochemical model for Loma Negra Formation deposition including some redox indicators. (A) Lower green facies; (B) Upper black facies.

supports that the coupled $\delta^{34}S$ values in both, sulfide and sulfate can be the result of an active sulfate reduction under very low sulfate concentrations. Bacterial sulfate reduction alone (given the low amount of sulfides) would hardly consume the bottom water sulfate to explain the very positive sulfur isotope ratios of both pyrite and sulfate. Complete consumption of the sulfate supply limits the ^{32}S preference inherent to bacterial sulfate reduction. If the basin was stratified, the export of sulfate to the deep ocean was certainly low and makes the production of isotopically heavy pyrites possible through bacterial sulfate reduction (e.g. Ries et al., 2009). A large dissolved organic carbon reservoir is also required in a stratified basin. The parallel positive excursion in both $\delta^{13}C_{car}$ and $\delta^{13}C_{ker}$ is explained by high bioproductivity which should enhance either, oxygenation of surface waters and oxygen-depletion in bottom waters, thereby reinforcing water-column stratification. High productivity is confirmed by the highest $\Delta^{13}C_{car\text{-}ker}$ values recorded here. High bioproductivity and concomitant oxygenation of surface environments has been postulated for the correlative member of the Polanco Formation (Arroyo del Soldado Group) on the basis of chromium isotopes (Frei et al., 2011). Summing up, the sulfur source for ^{34}S-enriched pyrites was the anoxic bottom waters characterized by intense sulfate reduction coupled to low seawater sulfate concentrations.

Conversely, the less ^{34}S-enriched CAS was most probably derived from surface waters where sulfate concentration from a weathering input should be higher than in the deep ocean. Alternatively, direct oxidation of deep water sulfide could also take place in the redox chemocline producing ^{34}S-depleted sulfate. No fractionation is known to occur during oxidation of sulfide (Canfield, 2001) and therefore explains the nearly similar sulfur isotopic composition of coeval CAS and sulfide (Hurtgen et al., 2006).

A shift in the redox chemistry of the ocean is evident at the transition from the green to black micritic limestones of Loma Negra Formation. While the pyritic green limestones are characterized by high [Fe], the black limestones record an important organic matter content (Fig. 8). Reducing conditions were most probably maintained as reflected by high concentrations in some redox-sensitive elements even if they were sometimes restricted to the water–sediment interface. The Mn/Al ratio along the SBG section remains below the average carbonate value supporting also reducing conditions. However, the scarcity of authigenic pyrite (only very small anhedral disseminated crystals) in the black micritic limestones appears as the critical clue. The environment recorded in the black limestones is shallower than that inferred for the green limestones and could be out of the influence of a water

redox chemocline. Aggradation of the carbonate platform in a restricted lagoon, as was interpreted by Poiré (1987, 1993), could have contributed to elevate the level of the sea bed above the redox chemocline (Fig. 8). In consequence, pyrite formation was inhibited in sediments not exposed to the chemocline as explained above. However, when noticed, the sedimentary pyrite was most probably the product of sulfur reoxidation due to the exposition of the platform to the aerobic conditions (Ries et al., 2009). The Ce anomaly in the black micritic facies is markedly negative and considering that this parameter is a reliable proxy for constraining redox conditions in seawater, it suggests that oxidizing conditions were present in the water column (Fig. 8). However, the concentrations of TE are more probably reflecting reducing conditions in the sediment. The most plausible explanation is that these TE were linked to the organic matter.

The validity of these data in the global chemostratigraphic record is given by the isotopic correlation of C and Sr in all sedimentary successions encompassed in the SW-Gondwana. The lagoon represented by the black micritic limestones of Loma Negra Formation, has a C and Sr isotopic record tracking all variations reported in the Ediacaran sea. (Gómez Peral et al., 2007, 2012; Gaucher et al., 2009).

5.3. Microbial diversity in the Loma Negra Formation

The biomarker distribution in the micritic limestones of Loma Negra Formation points to a diverse microbial community including primary producers such as cyanobacteria (e.g. terminally-branched monomethylalkanes, hopanoid distribution), phototrophic bacteria (e.g. acyclic isoprenoids $C_{<21}$), green bacteria (e.g. n-$C_{18} \gg$ Ph) and some methanogenic bacteria (e.g. 2-methyloctadecane). The signature of heterotrophy was also identified in this facies by the occurence of specific biomarkers (2-methylpentadecane and 2-methylhexadecane). Therefore, the green facies of Loma Negra limestones may include a contribution of sulfate reducing bacteria considering the abundance of pyrite. The occurrence of green non-sulfur bacteria (*Chloroflexus*) was suggested by the predominance of n-C_{18} over phytane (e.g. sample AR04: Ph/n-C_{18} = 0.49). The inferred microbial ecosystem represented in limestones of Loma Negra Formation strongly supports the existence of a redox boundary in a stratified ocean and/or at the water–sediment interface. The record of redox sensitive elements, the Ce anomaly, the $\sum$REE contents and particularly the sulfur isotopic composition of these samples are all in line with this interpretation.

Benthic skeletal fossils such as *Cloudina* were identified in these facies but their preservation is poor (Gaucher et al., 2005). They were reported in the basal micritic limestones but they do not occur in life-position. Thus, the occurrence of this fauna does not constrain oxygenic conditions of the basal facies of Loma Negra Formation.

The $\Delta^{13}C_{car\text{-}ker}$ ratio can be used to estimate the local photosynthetic fractionation in the Loma Negra Formation. The green micritic limestones are characterized by unsteady $\Delta^{13}C_{car\text{-}ker}$ values exhibiting high variations. This trend can reflect a change of the prevailing organisms using different metabolic pathways to fix carbon. The sample exhibiting a clear predominance of n-C_{18} over Ph which is interpreted as reflecting an input of green non-sulfur bacteria, correspond with that having the lowest $\Delta^{13}C_{car\text{-}ker}$ values. These organisms, using a less ^{13}C-fractionating pathway for CO_2 fixation, lead to biomass enriched in ^{13}C. Otherwise, the $\Delta^{13}C_{car\text{-}ker}$ values reported for most of the Loma Negra limestones are consistent with carbon isotope fractionation by oxygenic photoautotrophs.

6. Conclusions

The existence of a euxinic setting in the Ediacaran ocean in the aftermath of Neoproterozoic glaciations (i.e. the last glaciation known as “Gaskiers” could be assigned to the Colombo diamictite at the base of Cerro Largo Formation; Gaucher and Poiré, 2009) was evidenced by the sulfur isotopic composition of coeval CAS and sulfide in the Loma Negra Formation. The ^{34}S enrichments in sulfides exceeding coeval $\delta^{34}S_{CAS}$ values in the green micritic limestones of Loma Negra Formation is viewed as a combined product of globally low seawater sulfate, high rates of bacterial sulfate reduction, and sulfate limitations under a stratified water column inherited from glaciations, particularly the lower water layer. The ^{34}S-enriched pyrites were plausibly derived from the anoxic bottom waters while the relatively ^{34}S-depleted CAS may have come from surface waters or be produced in the redox chemocline by direct oxidation of sulfides. Diverse geochemical proxies in the green limestones of Loma Negra Formation are pointed to reducing conditions during its deposition and/or early diagenesis (e.g. higher concentrations of Fe, Mo, Zn and REE, the occurrence of authigenic isotopically-enriched pyrite and a molecular-inferred microbial ecosystem most probably including green non-sulfur bacteria).

Water column stratification was favourable to the stockage of large amounts of nutrients in the deep ocean. During upwelling periods, the export of the nutrient-rich waters may have triggered an important bioproductivity in surface waters. Positive $\delta^{13}C_{car}$ excursions highlight the increase in primary productivity. The local photosynthetic fractionation during de deposition of the green limestones was highly variable as indicated by the $\Delta^{13}C_{car\text{-}ker}$ ratio. The unsteady $\Delta^{13}C_{car\text{-}ker}$ values reflect changes in the primary biomass using different photosynthetic mechanisms to fix carbon. The lowest $\Delta^{13}C_{car\text{-}ker}$ values coincided with a biomarker distribution interpreted as the signature of green non-sulfur bacteria using a less ^{13}C fractionation pathway.

The black micritic limestones of Loma Negra Formation were most probably deposited under oxidizing conditions in the water column as revealed by a clear negative Ce anomaly. These sediments were deposited in a restricted lagoon allowing the aggradation of the carbonate platform and thus elevating the sea bed above the redox chemocline. However, reducing conditions were maintained into the sediments during early burial diagenesis as evidenced by the record of trace elements and molecular biomarkers. A hopanes distribution with maxima in the C_{29} hopane indicates an anoxic source–rock depositional environment.

Acknowledgements

We would like to thank Claudio Gaucher and Hartwig Frimmel for the discussion and constructive comments on a previous version. We would also like to thank José M. Canalicchio from Cementos Avellaneda SA for their logistic coperation and geological field discussions. This study was financial supported by the Swiss National Science Foundation, the University of Lausanne and the Société Académique Vaudoise.

References

Bagnoud, M. 2010. Environmental changes in the aftermath of Neoproterozoic glaciations: a biogeochemical study of sediments from SW-Gondwana. Ph.D Thesis, Faculté de Geosciences et Environnement, Université de Lausanne, pp. 1–200.

Boggiani, P.C., Gaucher, C., Sial, A.N., Babinski, M., Simon, C.M., Riccomini, C., Ferreira, V.P., Fairchild, T.R., 2010. Chemostratigraphy of the Tamengo Formation (Corumbá Group, Brazil): a contribution to the calibration of the Ediacaran carbon-isotope curve. Precambrian Research 182, 382–401.

Borrello, A.V., 1966. Trazas, restos tubiformes y cuerpos fósiles problemáticos de la Formacion La Tinta, Sierras Septentrionales de la Provincia de Buenos Aires.

Paleontografía Bonaerense, Fascículo 5. Comisión de Investigaciones Científicas, Provincia de Buenos Aires, La Plata, Argentina, pp. 1–42.
Brassell, S.C., Wardroper, A.M.K., Thomson, I.D., Maxwell, J.R., Eglinton, G., 1981. Specific acyclic isoprenoids as biological markers of methanogenic bacteria in marine sediments. Nature 290, 693–696.
Burdett, J.W., Arthur, M.A., Richardson, M., 1989. A Neogene seawater sulfur isotope age curve from calcareous pelagic microfossils. Earth and Planetary Science Letters 94, 189–198.
Canfield, D.E., 2001. Biogeochemistry of sulfur isotopes. Reviews in Mineralogy and Geochemistry 43, 607–636.
Canfield, D.E., Thamdrup, B., 1994. The production of ^{34}S-depleted sulfide during bacterial disproportionation of elemental sulfur. Science 266, 1973–1975.
Cingolani, C.A., Rauscher, R., Bonhomme, M., 1991. Grupo La Tinta (Precámbrico y Paleozoico inferior) provincia de Buenos Aires, República Argentina. Nuevos datos geocronológicos y micropaleontológicos en las sedimentitas de Villa Cacique, partido de Juarez. Revista Técnica de YPFB 12, 177–191.
Cingolani, C., 2011. The Tandilia System of Argentina as a southern extension of the Río de la Plata craton: an overview. International Journal of Earth Sciences 100, 221–242.
Dalla Salda, L., Spalletti, L., Poiré, D., De Barrio, R., Echebeste, H., Benialgo, A., 2006. Tandilia. Serie Correlación Geológica 21, 17–46.
Fölling, P.G., Frimmel, H.E., 2002. Chemostratigraphic correlation of carbonate successions in the Gariep and Saldania Belts, Namibia and South Africa. Basin Research 14, 69–88.
Frei, R., Gaucher, C., Døssing, L.N., Sial, A.N., 2011. Chromium isotopes in carbonates – a tracer for climate change and for reconstructing the redox state of ancient seawater. Earth and Planetary Science Letters 312, 114–125.
Frimmel, H.E., 2010. On the reliability of stable carbon isotopes for Neoproterozoic chemostratigraphic correlation. Precambrian Research 182 (4), 239–253.
Gaucher, C., Boggiani, P.C., Sprechmann, P., Sial, A.N., Fairchild, T.R., 2003. Integrated correlation of the Vendian to Cambrian Arroyo del Soldado and Corumbá Groups (Uruguay and Brazil): palaeogeographic, palaeoclimatic and palaeobiologic implications. Precambrian Research 120, 241–278.
Gaucher, C., Sial, A.N., Blanco, G., Sprechmann, P., 2004. Chemostratigraphy of the lower Arroyo del Soldado Group (Vendian, Uruguay) and palaeoclimatic implications. Gondwana Research 7 (3), 715–730.
Gaucher, C., Poiré, D.G., Gómez Peral, L., Chiglino, L., 2005. Litoestratigrafía, bioestratigrafía y correlaciones de las sucesiones sedimentarias del Neoproterozoico-Cámbrico del Cratón del Rio de la Plata (Uruguay y Argentina). Latin American Journal of Sedimentology and Basin Analysis 12 (2), 145–160.
Gaucher, C., Finney, S.C., Poiré, D.G., Valencia, V.A., Grove, M., Blanco, G., Pamoukaghlián, K., Peral, L.G., 2008. Detrital zircon ages of Neoproterozoic sedimentary successions in Uruguay and Argentina: insights into the geological evolution of the Río de la Plata Craton. Precambrian Research 167, 150–170.
Gaucher, C., Poiré, D., 2009. Palaeoclimatic events. Neoproterozoic–Cambrian evolution of the Río de la Plata Palaeocontinent. In: Gaucher, C., Sial, A.N., Halverson, G.P., Frimmel, H.E. (Eds.), Neoproterozoic–Cambrian Tectonics, Global Change and Evolution: A Focus on Southwestern Gondwana. Developments in Precambrian Geology, vol. 16. Elsevier, Amsterdam, pp. 123–130.
Gaucher, C., Sial, A.N., Poiré, D., Gómez-Peral, L., Ferreira, V.P., Pimentel, M.M., 2009. Chemostratigraphy. Neoproterozoic–Cambrian evolution of the Río de la Plata Palaeocontinent. In: Gaucher, C., Sial, A.N., Halverson, G.P., Frimmel, H.E. (Eds.), Neoproterozoic–Cambrian tectonics, Global Change and Evolution: A Focus on Southwestern Gondwana. Developments in Precambrian Geology, vol. 16. Elsevier, Amsterdam, pp. 115–122.
Gelin, F., De Leeuw, J.W., Sinninghe Damsté, J.S., Derenne, S., Metzger, P., 1994. The similarity of chemical structures of soluble aliphatic polyaldehyde and insoluble algaenan in the green microalga *Botryococcus braunii* race A as revealed by analytical pyrolysis. Organic Geochemistry 21, 423–435.
Goldberg, T., Poulton, S.W., Strauss, H., 2005. Sulfur and oxygen isotope signatures of late Neoproterozoic to early Cambrian sulphate, Yangtze Platform, China: diagenetic constraints and seawater evolution. Precambrian Research 137, 223–241.
Gómez Peral, L.E., Poiré, D.G., Strauss, H., Zimmermann, U., 2007. Chemostratigraphy and diagenetic constraints on Neoproterozoic carbonate successions from the Sierras Bayas Group, Tandilia System, Argentina. Chemical Geology 237, 109–128.
Gómez Peral, L.E., Sial, A.N., Poiré, D.G., Arrouy, J., Canalicchio, J.M., 2010. C–O isotopes of the Ediacarian Loma Negra Formation in Barker area, Tandilia System, Argentina: diagenetic implications. In: 18th International Sedimentological Congress, Abstract 398, Mendoza, Argentina.
Gómez Peral, L.E., Raigemborn, M.S., Poiré, D.G., 2011. Petrología y evolución diagenética de las facies silicoclásticas del Grupo Sierras Bayas, Sistema de Tandilia, Argentina. Latin American Journal of Sedimentology and Basin Analysis 18, 3–41.
Gómez Peral, L.E., Sial, A.N., Poiré, D.G., Kaufman, A.J., Arrouy, J., 2012. C–O–Sr isotope stratigraphy of the Neoproterozoic carbonate Successions of the Sierras Bayas Group, Río de La Plata Craton, Argentina: palaeoclimatic implications. In: The Neoproterozoic Era: Evolution, Glaciations, Oxygenation, 19–21 September 2012, Londres, Inglaterra, Abstract Book, pp. 128–129.
Habicht, K.S., Gade, M., Thamdrup, B., Berg, P., Canfield, D.E., 2002. Calibration of sulfate levels in the Archean ocean. Science 298, 2372–2374.
Halverson, G.P., Wadeb, B.P., Hurtgenc, M.T., Barovicha, K.M., 2010. Neoproterozoic chemostratigraphy. Precambrian Research 182, 337–350.
Hurtgen, M.T., Arthur, M.A., Suits, N.S., Kaufman, A.J., 2002. The sulfur isotopic composition of Neoproterozoic seawater sulfate: implications for a snowball Earth? Earth and Planetary Science Letters 203, 413–429.
Hurtgen, M.T., Arthur, M.A., Prave, A.R., 2004. The sulfur isotope composition of carbonate-associated sulfate in Mesoproterozoic to Neoproterozoic carbonates from Death Valley, California. In: Amend, J.P., Edwards, K.J., Lyons, T.W. (Eds.), Sulfur Biogeochemistry—Past and Present, vol. 379. Geological Society of America Special Paper, pp. 177–194.
Hurtgen, M.T., Arthur, M.A., Halverson, G.P., 2005. Neoproterozoic sulfur isotopes, the evolution of microbial sulfur species, and the burial efficiency of sulfide as sedimentary pyrite. Geology 33, 41–44.
Hurtgen, M.T., Halverson, G.P., Arthur, M.A., Hoffman, P.F., 2006. Sulfur cycling in the aftermath of a 635-Ma snowball glaciation: evidence for a syn-glacial sulfidic deep ocean. Earth and Planetary Science Letters 245, 551–570.
Iñiguez Rodriguez, A.M., 1999. La Cobertura Sedimentaria de Tandilia. In: Caminos, R. (Ed.), Geología Argentina, Anales 29. SEGEMAR, Buenos Aires, pp. 101–106.
Iñiguez Rodriguez, A.M., Zalba, P.E., 1974. Nuevo nivel de arcilitas en la zona de Cerro Negro, Partido de Olavarria, Provincia de Buenos Aires. Anales del LEMIT 264, 95–100, Serie 2.
Kaufman, A.J., Corsetti, F.A., Varni, M.A., 2007. The effect of rising atmospheric oxygen on carbon and sulfur isotope anomalies in the Neoproterozoic Johnnie Formation, Death Valley, USA. Chemical Geology 237, 47–63.
Kaufman, A.J., Hebert, C.L., 2003. Stratigraphic and radiometric constraints on rift-related volcanism, terminal Neoproterozoic glaciation, and animal evolution. In: Abstract Programs – Geological Society of America, vol. 35, p. 516.
Kawashita, K., Varela, R., Cingolani, C., Soliani Jr., E., Linares, E., Valencio, S.A., Ramos, A.V., Do Campo, M., 1999. Geochronology and chemostratigraphy of La Tinta Neoproterozoic sedimentary rocks, Buenos Aires Province, Argentina. In: II South American Symposium on Isotope Geology, Brazil, pp. 403–407.
Lyons, T.W., Werne, J.P., Hollander, D.J., Murray, R.W., 2003. Contrasting sulfur geochemistry and Fe/Al and Mo/Al ratios across the last oxic-to-anoxic transition in the Cariaco Basin, Venezuela. Chemical Geology 195, 131–157.
Lyons, T.W., Gellatly, A.M., McGoldrick, P.J., Kah, L.C., 2006. Proterozoic sedimentary exhalative (SEDEX) deposits and links to evolving global ocean chemistry. In: Kesler, S.E., Ohmoto, H. (Eds.), Evolution of Early Earth's Atmosphere, Hydrosphere, and Biosphere—Constraints from Ore Deposits, vol. 198. Geological Society of America Memorials, pp. 169–184.
Martínez, J.C., Dristas, J.A., 2007. Paleoactividad hidrotermal en la discordancia entre el Complejo Buenos Aires y la Formación La Tinta en el área de Barker, Tandilia. Revista de la Asociación Geológica Argentina 62, 375–386.
McFadden, K.A., Huang, J., Chu, X., Jiang, G., Kaufman, A.J., Zhou, C., Yuan, X., Xiao, S., 2008. Pulsed oxidation and biological evolution in the Ediacaran Doushantuo Formation. Proceedings of the National Academy of Sciences 105, 3197–3202.
Misi, A., Kaufman, A.J., Veizer, J., Powis, K., Azmy, K., Boggiani, P.C., Gaucher, C., Teixeira, J.B.G., Sanches, A.L., Iyer, S.S.S., 2007. Chemostratigraphic correlation of Neoproterozoic successions in South America. Chemical Geology 237, 143–167.
Oshima, M., Ariga, T., 1975. Omega-cyclohexyl fatty acids in acidophilic thermophilic bacteria. Studies on their presence, structure, and biosynthesis using precursors labeled with stable isotopes and radioisotopes. Journal of Biological Chemistry 250, 6963–6968.
Ourisson, G., Albrecht, P., 1992. Hopanoids 1. Geohopanoids: the most abundant natural products on Earth. Accounts of Chemical Research 25, 398–402.
Peters, K.E., Walters, C.C., Moldowan, J.M., 2005. The Biomarker Guide, vol. 1. Cambridge University Press, Cambridge, 471 p.
Poiré, D.G., 1987. Mineralogía y sedimentología de la Formación Sierras Bayas en el núcleo septentrional de las sierras homónimas, Partido de Olavarría, Provincia de Buenos Aires. Ph.D Thesis, Facultad de Ciencias Naturales y Museo, Universidad Nacional de La Plata, pp. 1–271.
Poiré, D.G., 1993. Estratigrafía del Precámbrico sedimentario de Olavarría, Sierras Bayas, provincia de Buenos Aires, Argentina. In: XII Congreso Geológico Argentino y II Congreso Exploración de Hidrocarburos Actas II, Mendoza, pp. 1–11.
Poiré, D.G., 2004. Sedimentary history of the Neoproterozoic of Olavarría, Tandilia System, Argentina: new evidence from their sedimentary sequences and unconformities—a snowball Earth or a phantom glacial? In: 1st Symposium on Neoproterozoic–Early Paleozoic Events in SW-Gondwana, Extended abstract: 46–48, San Pablo, Brasil.
Poiré, D.G., Spalletti, L.A., del Valle, A., 2003. The Cambrian–Ordovician siliciclastic platform of the Balcarce Formation (Tandilia System, Argentina): facies, trace fossils, palaeoenvironments and sequence stratigraphy. Geologica Acta 1, 41–60.
Poiré, D.G., Spalletti, L.A., 2005. La cubierta sedimentaria precámbrica-paleozoica inferior del Sistema de Tandilia. In: de Barrio, R.E., Etcheverry, R.O., Caballé, M.F., Llambías, E. (Eds.), Geología y Recursos Minerales de la Provincia de Buenos Aires. Relatorio del XVI Congreso Geológico Argentino, La Plata. , pp. 51–68.
Poiré, D.G., Gómez Peral, L., Bertolino, S., Canalicchio, J.M., 2005. Los niveles con pirofilita de la Formación Villa Mónica, Precámbrico de Olavarría, Sistema de Tandilia, Argentina. In: XVI Congreso Geológico Argentino, Actas II, pp. 863–866.
Poiré, D.G., Gaucher, C., 2007. Lithostratigraphy and correlations of two Neoproterozoic basins from the Río de la Plata Craton, SWGondwana. In: III Symposium on Neoproterozoic–Early Palaeozoic Events in southwestern Gondwana, Programme and Short Papers, Stellenbosch, pp. 23–27.
Poiré, D.G., Gaucher, C., 2009. Neoproterozoic–Cambrian eolution of the Rio de la Plata Palaeocontinent: Ithostratigraphy. In: Gaucher, C., Sial, A.N., Halverson, G.P., Frimmel, H.E. (Eds.), Neoproterozoic–ambrian Tectonics, Global Change and Evolution: A Focus on Southwestern Gondwana. Developments in Precambrian Geology, vol. 16. Elsevier, Amsterdam, pp. 87–102.
Porada, H., Bouougri, E., 2008. Neoproterozoic trace fossils vs. microbial mat structures: examples from the Tandilia Belt of Argentina. Gondwana Research 13, 480–487.

Rapela, C.W., Pankhurst, R.J., Casquet, C., Fanning, C.M., Baldo, E.G., González-Casado, J.M., Galindo, C., Dahlquist, J., 2007. The Río de la Plata Craton and the assembly of SW Gondwana. Earth Science Reviews 83, 49–82.

Rapalini, A.E., Trindade, R.I., Poiré, D.G., 2013. The La Tinta pole revisited: Paleomagnetism of the Neoproterozoic Sierras Bayas Group (Argentina) and its implications for Gondwana and Rodinia. Precambrian Research 224, 51–70.

Reuschel, M., Melezhik, V.A., Strauss, H., 2012. Sulfur isotopic trends and iron speciation from the c. 2.0 Ga Pilgujärvi Sedimentary Formation, NW Russia. Precambrian Research 196–197, 193–203.

Ries, J.B., Fike, D.A., Pratt, L.M., Lyons, T.W., Grotzinger, J.P., 2009. Superheavy pyrite ($\delta^{34}S_{pyr} > \delta^{34}S_{CAS}$) in the terminal Proterozoic Nama Group, southern Namibia: a consequence of low seawater sulfate at the dawn of animal life. Geology 37, 743–746.

Schoell, M., 1984. Recent advances in petroleum isotope geochemistry. Organic Geochemistry 6, 645–663.

Schulze, T., Michaelis, W., 1990. Structure and origin of terpenoid hydrocarbons in some German coals. In: Organic Geochemistry, Proceedings of the 14th International Meeting on Organic Geochemistry, vol. 16, pp. 1051–1058.

Shen, B., Xiao, S., Kaufman, A.J., Bao, H., Zhou, C., Wang, H., 2008. Stratification and mixing of a post-glacial Neoproterozoic ocean: evidence from carbon and sulfur isotopes in a cap dolostone from northwest China. Earth and Planetary Science Letters 265, 209–228.

Shiea, J., Brassell, S.C., Ward, D.M., 1990. Mid-chain branched mono- and dimethyl alkanes in hot spring cyanobacterial mats: A direct biogenic source for branched alkanes in ancient sediments? Organic Geochemistry 15, 223–231.

Shiea, J., Brassel, S.C., Ward, D.M., 1991. Comparative analysis of extractable lipids in hot spring microbial mats and their component photosynthetic bacteria. Organic Geochemistry 17, 309–319.

Shields, G.A., Kimura, H., Yang, J., Gammon, P., 2004. Sulfur isotopic evolution of Neoproterozoic–Cambrian seawater: new francolite-bound sulphate S data and critical appraisal of the existing record. Chemical Geology 204, 163–182.

Spangenberg, J.E., Herlec, U., 2006. Hydrocarbon biomarkers in the Topla-Mezica zinc–lead deposits, Northern Karavanke/Drau Range, Slovenia: paleoenvironment at the site of ore formation. Economic Geology 101, 997–1021.

Spangenberg, J.E., Frimmel, H.E., 2001. Basin-internal derivation of hydrocarbons in the Witwatersrand Basin, South Africa: evidence from bulk and molecular $\delta^{13}C$ data. Chemical Geology 173, 339–355.

Spangenberg, J.E., Macko, S.A., 1998. Organic geochemistry of the San Vicente zinc–lead district, eastern Pucará Basin, Peru. Chemical Geology 146, 1–23.

Strauss, H., 2002. The isotopic composition of Precambrian sulphides: seawater chemistry and biological evolution. In: Altermann, W., Corcoran, P.L. (Eds.), Precambrian Sedimentary Environments: A Modern Approach to Ancient Depositional Systems. Blackwell Science, Oxford, pp. 67–105 (Special Publication Number 33 of the International Association of Sedimentologists).

Taylor, S.R., McLennan, S.M., 1985. The Continental Crust: Its Composition and Evolution. Blackwell, Oxford, 312 p.

Ten Haven, H.L., de Leeuw, J.W., Sinninghe Damste, J.S., Schenck, P.A., Palmer, S.E., Zumberge, J.E., 1988. Application of biological markers in the recognition of palaeo hypersaline environments. In: Kelts, K., Fleet, A., Talbot, M. (Eds.), Lacustrine Petroleum Source Rocks, vol. 40. Geological Socity of London Special Publication, pp. 123–140.

Turekian, K.K., Wedepohl, K.H., 1961. Distribution of the elements in some major units of the Earth's crust. Geological Society of America Bulletin 72, 175–192.

Veizer, J., 1983. Trace elements and isotopes in sedimentary carbonates. Reviews in Mineralogy and Geochemistry 11, 265–299.

Volkman, J.K., Johns, R.B., Gillan, F.T., Perry, G.J., Bavor, H.J., 1980. Microbial lipids of an intertidal sediment—I. Fatty acids and hydrocarbons. Geochimica et Cosmochimica Acta 44, 1133–1143.

Zalba, P.E., 1979. Clay deposits of Las Aguilas Formation, Barker, Buenos Aires province, Argentina. Clays and Clay Minerals 27 (6), 433–439.

Zalba, P.E., Poiré, D.G., Andreis, R.R., Iñiguez Rodriguez, A.M., 1992. Precambrian and Lower Paleozoic records and paleosurfaces of the Tandilia System, Buenos Aires Province, Argentina. In: Schmitt, J.M., Gall, Q. (Eds.), Mineralogical and Geochemical Records of Paleoweathering, vol. 18. Memoire des Sciences de la Terre, pp. 93–113.